Optimization of multistage membrane distillation system for treating shale gas produced water

Alba Carrero-Parreño[a,], Viviani C. Onishi[a], Rubén Ruiz-Femenia[a,b], Raquel Salcedo-Díaz[a,b*], José A. Caballero[a,b], Juan A. Reyes-Labarta[a,b]

[a]*Institute of Chemical Process Engineering, University of Alicante, Ap Correos 99, Alicante 03080, Spain*

[b]*Department of Chemical Engineering, University of Alicante, Ap Correos 99, Alicante 03080, Spain*

**** Corresponding author at.*** *Institute of Chemical Process Engineering, University of Alicante, Ap Correos 99, Alicante 03080, Spain. Phone: +34 965903400.*

E-mail: raquel.salcedo@ua.es

ABSTRACT

Thermal membrane distillation (MD) is an emerging technology to desalinate high-salinity wastewaters, including shale gas produced water to reduce the corresponding water footprint of fracturing operations. In this work, we introduce a rigorous optimization model with energy recovery for the synthesis of multistage direct contact membrane distillation (DCMD) system. The mathematical model (implemented in GAMS software) is formulated via generalized disjunctive programming (GDP) and mixed-integer nonlinear programming (MINLP). To maximize the total amount of water recovered, the outflow brine is fixed close to salt saturation conditions (300 $g \cdot kg^{-1}$ water) approaching zero liquid discharge (ZLD).

A sensitivity analysis is performed to evaluate the system's behavior under different uncertainty sources such as the heat source availability and inlet salinity conditions. The results emphasize the applicability of this promising technology, especially with low steam cost or waste heat, and reveal variable costs and system configurations depending on inlet conditions. For a produced water salinity ranging from 150 $g \cdot kg^{-1}$ water to 250 $g \cdot kg^{-1}$ water based on Marcellus play, an optimal treating cost are between 11.5 and 4.4 US$ m^{-3} is obtained when using low-cost steam. This cost can decrease to 2.8 US$ m^{-3} when waste heat from shale gas operations is used.

Keywords: shale gas water, zero liquid discharge (ZLD), membrane distillation, optimal configuration

1. Introduction

Unconventional shale gas is an energy resource with the potential to change the global energy market, particularly considering the continuous increase in the demand for energy on a worldwide scale (Department of Energy & Climate Change, 2013; Hammond and O'Grady, 2017; U.S. Energy Information Administration, 2017).

Shale gas trapped in shale formations is released by injecting large amounts of water (10,500 – 38,000 m^3 per well) under high pressure to fracture the impermeable rock (*hydraulic fracturing*) (Jacquet, 2014; Yang et al., 2014). Part of the injected fluid (10-40%) called *flowback water* is recovered containing total dissolved solids (TDS) ranging from 10,000 to 150,000 $mg \cdot L^{-1}$, taking from between a few days to a few weeks. The wastewater that is generated over the rest of the life of the well (10 - 30 years) is called *produced water*. The TDS concentration in long-term produced water can reach 250,000 $mg \cdot L^{-1}$ (U.S. Environmental Protection Agency, 2016).

Current water management strategies include disposal of wastewater via Class II disposal wells, transfer to a centralized water treatment facility (CWT) or, direct reuse in drilling subsequent wells. Direct reuse (without any treatment) in drilling subsequent wells is currently the most popular option due to its operational simplicity for contractors (Ruyle and Fragachan, 2015). However, as the number of drilled wells decrease, this practice becomes less attractive. Specifically, as can be seen in **Fig. 1**, the volume of fracturing fluid required to fracture new wells may be less than the volume of water generated by producing wells in the area. Consequently, operators must find a viable, sustainable and bearable wastewater management alternative when wastewater generation exceeds the water demand for fracturing.

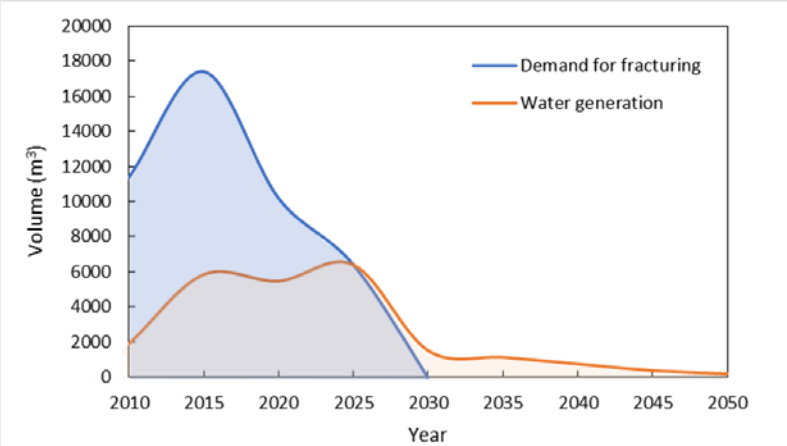

Fig. 1. Forecast of flowback and produced water generation and water demand over time (U.S. Environmental Protection Agency, 2016).

Shaffer et al. (2013) critically review mechanical vapor compression (MVC), membrane distillation (MD) and forward osmosis (FO) as suitable technologies to desalinate wastewater from shale gas operations. Onishi et al. (2017a, 2017b) developed a non-linear programming (NLP) model for the optimal design of single and multi-effect evaporation (SEE/MEE) systems with/without mechanical vapor recompression (MVR). Regarding FO optimization for treating shale gas water, Salcedo-Díaz et al. (2017) proposed a hybrid treatment combining FO with reverse osmosis (RO). Their solution shows a trade-off between fracturing water cost and freshwater consumption.

MD offers a great potential to treat shale gas water since the separation occurs below the normal boiling point of the inlet stream, therefore, it is possible to use waste heat to induce the separation (Ashoor et al., 2016; Drioli et al., 2015). This technology is especially advantageous in remote unconventional hydrocarbon extraction sites where electrical energy supply is not available and many waste heating sources are present, such as geothermal heat energy process facilities, or flaring (Chafidz et al., 2016; Deshmukh et al., 2018; Elsayed et al., 2015; Kim et al., 2017; Omkar R. Lokare et al., 2017). Furthermore, MD is also very attractive for this application due to its mobility,

modularity, and compactness, contrasting with conventional thermal desalination processes which involve a huge physical footprint (Silva et al., 2017).

Regarding membrane distillation optimization for the treatment of shale gas wastewater, Elsayed et al. (2015) have developed an optimization approach for treating flowback water by using direct contact membrane distillation (DCMD). However, they consider that waste energy is always available, hence there is no calculation of the energy cost or heat integration within the process streams. Moreover, in their optimization model, they do not consider process configuration design. Lokare et al., (2017) also evaluate the synergies and potential of DCMD technology for the treatment of shale gas water utilizing waste heat available from natural gas extraction. They simulate DCMD in ASPEN Plus and calibrate the model using laboratory-scale experiment. Then, the model is used to design and determine the operating parameters for a full-scale DCMD system. In a later work (Tavakkoli et al., 2017), the same authors highlighted the applicability of DCMD for treating shale gas water by evaluating the economic feasibility. Recently, Deshmukh et al. (2018) highlighted the advantages of MD for small-scale desalination applications and emphasized the benefits for desalinating shale gas water. However, they remark that the viability of MD as an energy-efficient treatment remains uncertain. Moreover, they mention the necessity of comparison techniques to obtain more reliable cost and process optimization.

To the best of our knowledge, there are no published optimization models for determining the optimal working conditions and membrane modules configuration for the MD treatment of shale gas produced water. For this reason, we introduce a mathematical model to optimize multistage membrane distillation systems (MDS) (including all potential membrane configurations in series and interconnections) for high-salinity conditions. The target of the MDS is to reduce the shale gas wastewater

volume as much as possible by producing concentrated saline water close to Zero Liquid Discharge (ZLD) - outlet flowrate water at near saturated conditions – maximizing at the same time the total water recovered at the minimum cost. The model is mathematically formulated as a Generalized Disjunctive Programming (GDP) problem (Trespalacios and Grossmann, 2014) and reformulated as a Mixed Integer Non-Linear Programming (MINLP) model to be solved using GAMS software (Rosenthal, 2016), seeking to minimize the total annualized cost of the process.

The main novelties of this study are: (1) development of an optimization model for MDS to attain close to ZLD conditions for the treatment of shale gas produced water; (2) optimization and design of full-scale membrane distillation systems coupled with heat recovery to determine the optimal system configuration and optimal working conditions; (3) application of the proposed model to real inlet flowrate and variable high-salinity to evaluate if the projected technology can be applied to desalinate produced water coming from different shale gas basins; and, (4) analysis of the economic viability of MD in shale gas operations.

The rest of the paper is organized as follows: section 2 describes the problem statement and the mathematical MINLP model; section 3 presents the case studies and section 4 the main results obtained. In addition, a critical appraisal for the sensitivity analysis is included; and section 5 summarizes the conclusions of the work.

2. Problem statement and mathematical model

The given parameters are: the defined wastewater feed stream (inlet mass flowrate, salinity, and temperature); the corresponding membrane characteristics (permeability and thickness); and, the cost of the membrane, pumps, heat exchangers and the utilities used (low-pressure steam and cooling water). The objective function considers the equipment’s annualized capital cost of expenditure and the operating costs related to

membrane labor, replacement, and energy demand. Additionally, improving process cost-effectiveness by achieving conditions close to ZLD reduces water footprint by reducing brine discharges and increasing water recovery.

The multistage superstructure proposed for treating produced water is shown in **Fig. 2**. The superstructure comprises *n* possible membrane modules in series and allows the possibility of various recycle connections. For instance, part of the concentrate obtained in stage two could be recycled in the same stage or could be sent to the first stage. There is only the possibility of recirculating the concentrated water to previous stages. On the other hand, if a membrane stage of the superstructure is not selected, the concentrated stream circulates through a bypass to the next stage.

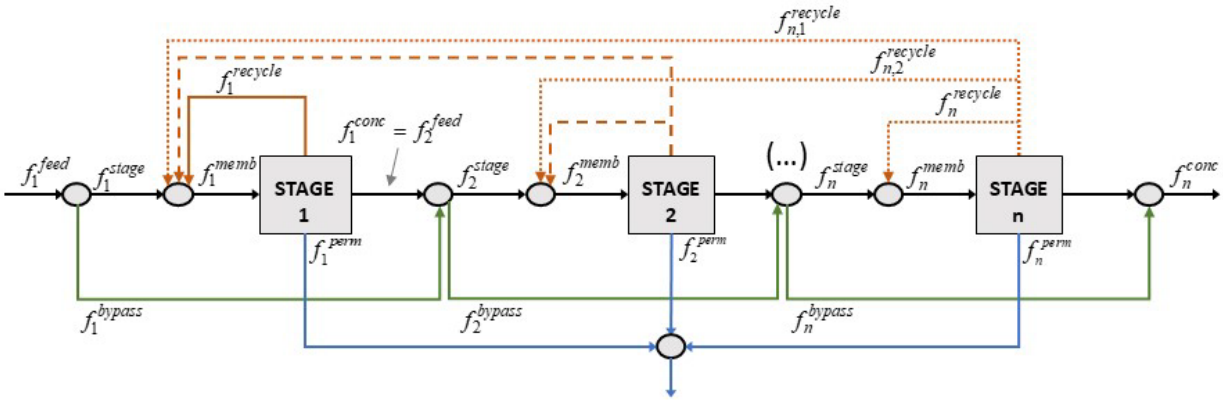

Fig. 2. Multistage Membrane Distillation superstructure for treating produced water from shale gas production.

DCMD is the configuration selected since it is recognized as the most suitable for purification of feed streams with non-volatile solutes and for small-scale desalination (Duong et al., 2015). **Fig. 3** shows the scheme of a DCMD module including heat recovery (Swaminathan et al., 2016). Each membrane module is composed of the following equipment: shell and tube heat exchanger, heater and cooler; polytetrafluoroethylene membranes with polypropylene support; centrifugal pumps and

storage tanks. The feed flowrate is heated before entering the membrane cell to induce the separation of salts and water. The driving force in DCMD is temperature difference between the inlet warm feed stream and ambient temperature of the permeate stream, which causes a difference of vapor pressures. To reduce the operational energy cost, a heat exchanger is used to preheat the inlet water with the hot permeate stream. Additionally, an external cooler is installed to cold down the recirculated permeate stream to generate a temperature difference across the membrane. To attain the specified outlet conditions, the concentrated stream leaving the membrane can also be recycled. Indeed, concentrate recycling is required for high recovery ratios (Lokare et al., 2018). The recirculated water of both sides of the membranes is stored in tanks installed in the feed and permeate loop, respectively. Finally, pumps are placed at the beginning of each stage and on the feed and permeate loop of each module to drive the recirculated water.

Throughout the work, we refer to heat exchangers when there is heat exchange between two streams within the system. Note that preheaters and coolers are also considered as heat exchangers but using external utilities.

Apart from the selection of the number of stages, the following decision variables are also calculated for each stage: membrane area; area and heating/cooling utility needed in the preheater and cooler; heat exchanger area; outlet concentration; recycle ratio; and operating temperatures.

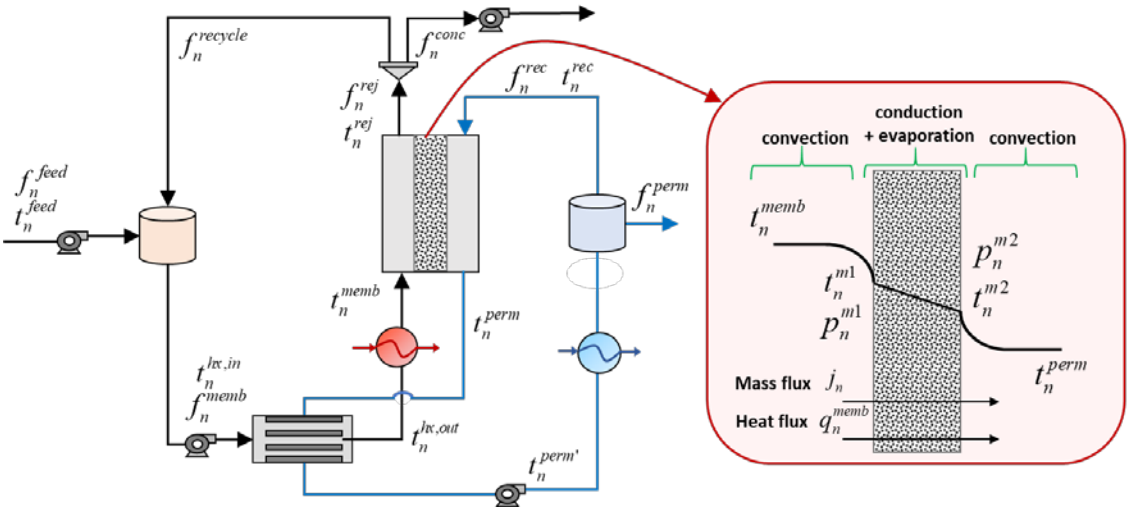

Fig. 3. Direct Contact Membrane Distillation module with heat recovery.

To simplify the mathematical formulation of the model, we have considered the following assumptions: steady state operation; heat losses in pipes, pumps, heater, and cooler are neglected; pressure drops in all thermal and mechanical equipment are negligible; vaporization takes place on the surface of the membrane; water with zero salinity goes through the membrane pores (permeate); and capital costs of mixers, splitters, pumps, tanks, and pipes are negligible.

The mathematical model, which includes equality and inequality constraints, logic propositions, data restriction and an objective function for the optimal multistage MDS, is formulated via Generalized Disjunctive Programming (GDP) and solved as a mixed-integer non-linear programming (MINLP) problem of the form:

$$\begin{aligned} &\textit{min}\ \text{Cost} \\ &s.t. \quad h(z) = 0 \\ &\qquad g(z) \le 0 \\ &z \in \mathrm{R}^n \end{aligned}$$

where z is a vector of continuous variables representing temperatures, flowrates and concentrations of the streams. In this case, the objective function represents the cost of the process. The equality set of constraints, $h(z) = 0$, are mass and energy balances and

the MD performance equations; and the set of inequalities, $g(z) \leq 0$, are the design specifications.

The optimization problem is modeled using total flows and salt composition as variables, which involves bilinear terms - the multiplication of two variables - in the salt water mass balances. These terms are one of the sources of the non-convexity; however, this representation is advantageous because the bounds of the variables can be easily determined. Note that throughout the mathematical model description, lower case letters are used for variables and capital letters for parameters.

The following data are assumed to be known:

F^{feed}	Inlet mass flowrate, kg·s^{-1}
T^{feed}	Inlet temperature, ºC
X^{feed}	Inlet salinity, g·kg^{-1}
X^{zld}	Outlet salinity, g·kg^{-1}
E	Membrane thickness, mm
B	Membrane permeability, kg (m^2·Pa·h)$^{-1}$
U^{preh}	Overall heat transfer coefficient of the preheater, kW (m^2 ºC)$^{-1}$
U^{cooler}	Overall heat transfer coefficient of the cooler, kW (m^2 ºC)$^{-1}$
T^{steam}	Steam low-pressure temperature, ºC
$T^{refrig,in}$	Cooling water inlet temperature, ºC
$T^{refrig,out}$	Cooling water outlet temperature, ºC
ΔT^{min}	Minimum temperature difference

2.1 Membrane distillation model

To develop the MINLP model, he following set is defined.

$$N = \{n / n \text{ is a stage of membrane in series}\}.$$

The simplest equations such as mass and salt balance around each membrane distillation unit, recycle splitter and mixer are detailed in Appendix A, Section A.1 to the interested reader.

The energy balance across the membrane can be evaluated as follows,

$$h_n^s(t_n^{memb}, x_n^{memb}) \cdot f_n^{memb} - h_n^s(t_n^{rej}, x_n^{rej}) \cdot f_n^{rej} = a_n^{memb} \cdot q_n^{memb} \quad \forall n \in N \quad (1)$$

$$h_n^p(t_n^{perm}) \cdot \left(f_n^{rec} + f_n^{perm} \right) - h_n^p(t_n^{rec}) \cdot f_n^{rec} = a_n^{memb} \cdot q_n^{memb} \quad \forall n \in N$$

(2)

where, a_n^{memb} and q_n^{memb} represent the membrane area and the heat transfer flux through the membrane. h_n^s and h_n^p are the specific enthalpies of saline water and permeate calculated at the specified conditions, correspondingly. Their values are calculated by the following rigorous correlations,

$$h_n^s = -15970 + 4.105 \cdot t_n + 8924 \cdot x_n - 3.709 \cdot t_n \cdot x_n + 84.77 \cdot x_n^2 \quad \forall n \in N$$

(3)

$$h_n^p = -15970 + 4.1178 \cdot t_n \quad \forall n \in N$$

(4)

where t_n and x_n are the corresponding temperature and composition.

These correlations have been generated using the maxmin approach – maximize the minimum distance between two sample points - considering temperature ranging from 0 ºC to 100 ºC, and brine salinity between 0 to 400 g·kg^{-1} water. Aspen HYSYS® simulator has been used to obtain the specific enthalpies by using the thermodynamic package NRTL electrolytes.

It is important to highlight that these rigorous correlations are crucial to simulate the real behavior of the MDS since the specific enthalpies in saline streams are significantly

dependent on temperature and composition. **Fig. 4** shows the surface plot of enthalpy as a function of salinity and temperature and the relative error obtained for each point.

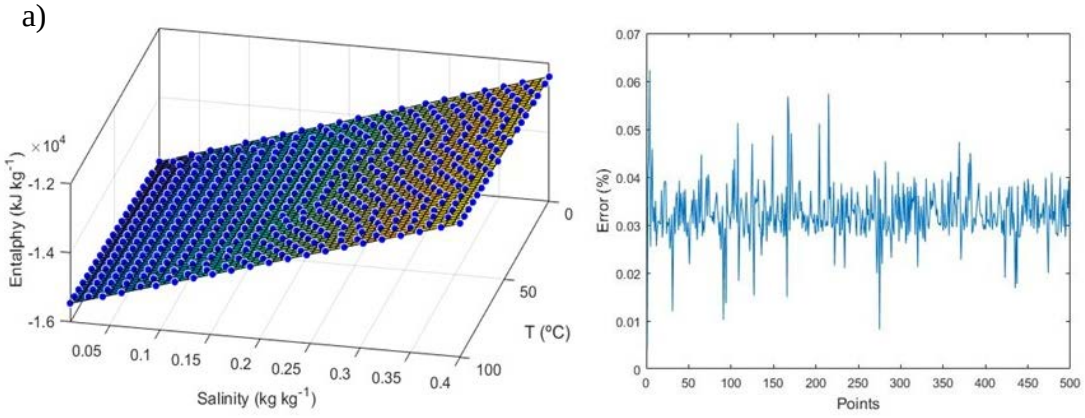

Fig. 4. (a) Surface plot of enthalpy as a function of salinity and temperature and (b) relative error.

The membrane area is calculated by **Eq. (5)**.

$$a_n^{memb} \cdot j_n = f_n^{perm} \qquad \forall n \in N$$

(5)

Where j_n is the permeate flux throughout the membrane calculated as proposed by Elsayed et al. (2014). Detailed description is provided in the **Appendix A, Section A.2**.

The heat transfer across each membrane, q_n^{memb}, is calculated by standard heat transfer models accounting the corresponding four contributions:

- Convection from the feed bulk to the membrane interface as expressed by **Eq. (6).**

$$q_n^{m1} = ht_n^{m1} \cdot (t_n^{memb} - t_n^{m1}) \qquad \forall n \in N \tag{6}$$

In which, ht_n^{m1} is the convective heat transfer coefficient given by the correlation described by **Eq. (7)** as a function of temperature and brine salinity. The produced water properties needed to calculate rigorously the convective heat transfer coefficient (density, viscosity, heat capacity and thermal conductivity) have been obtained from OLI's software (OLI Systems, 2010) using the thermodynamic package for electrolytes.

The physical properties correlations have been generated by considering temperature ranging from 40 ºC to 90 ºC, and brine salinity between 40 to 300 g·kg^{-1} water.

$$ht_n^{m1} = 2.61 - 4.96 \cdot x_n^{memb} + 0.03 \cdot t_n^{memb} \qquad \forall n \in N \tag{7}$$

- Conduction and water evaporation inside the membrane are given by **Eq. (8)**.

$$q_n^{memb} = ht_n^{cond} \cdot (t_n^{m1} - t_n^{m2}) + hv_n \cdot j_n \qquad \forall n \in N \tag{8}$$

hv_n is the water latent heat of vaporization. The conduction heat transfer coefficient, ht_n^{cond}, is defined by **Eq. (9)**.

$$ht_n^{cond} \cdot E = k_n \qquad \forall n \in N \tag{9}$$

In which, E is the thickness of the membrane and k_n is its thermal conductivity given by the following correlation proposed by Elsayed et al. (2014)**,** where t_n is the average temperature between t_n^{memb} and t_n^{perm}:

$$k_n = 1.7 \cdot 10^{-7} \cdot t_n - 4 \cdot 10^{-5} \qquad \forall n \in N \tag{10}$$

- Convection from the membrane interface to the permeate bulk is calculated by **Eq. (11)**.

$$q_n^{m2} = ht_n^{m2} \cdot (t_n^{m2} - t_n^{perm}) \qquad \forall n \in N \tag{11}$$

In which, ht_n^{m2} is the convective heat transfer coefficient at the permeate side given by the correlation defined in **Eq. (12)**. The same procedure detailed before for the calculation of the convective heat transfer coefficient at the feed side is used. In this

case, the water salinity in the permeate side is equal to zero (salt-free), and the temperature range is considered to vary from 20 to 90 ºC.

$$h_n^{m2} = 0.004 \cdot t_n^{perm} + 2.8 \qquad \forall n \in N$$

(12)

At steady state, the overall heat transfer flux must be balanced (Hitsov et al., 2015; Yun et al., 2006):

$$q_n^{m1} = q_n^{memb} = q_n^{m2} \qquad \forall n \in N$$

(13)

To avoid inconsistent performance of the membrane modules and solutions without physical meaning, the following constraints that ensure suitable working conditions (i.e. outlet flow should not be higher than inlet flow) should be introduced in the model:

$$f_n^{rej} \leq f_n^{memb} \quad \forall n \in N \tag{14}$$

$$f_n^{conc} \leq f_n^{rej} \quad \forall n \in N \tag{15}$$

$$t_n^{m1} \leq t_n^{memb} \quad \forall n \in N \tag{16}$$

$$t_n^{m2} \leq t_n^{m1} \quad \forall n \in N \tag{17}$$

$$t_n^{perm} \leq t_n^{m2} \quad \forall n \in N \tag{18}$$

Finally, the following design specification is included to reach close to ZLD conditions at the end of the membrane system.

$$x_n^{rej} \geq X^{zld} \qquad n = |N| \tag{19}$$

2.2 Design equations for the preheater, cooler and heat exchanger

The energy required in the preheater is given by **Eq. (20)**,

$$q_n^{preh} = f_n^{memb} \cdot \left(h_n^s(t_n^{memb}, x_n^{memb}) - h_n^s(t_n^{hx,out}, x_n^{memb}) \right) \qquad \forall n \in N$$

(20)

where t_n^{memb} and $t_n^{hx,out}$ are the inlet membrane temperature and the outlet heat exchanger temperature, respectively.

The heat transfer area is defined by the following equation:

$$a_n^{preh} \cdot U^{preh} \cdot lmtd_n^{preh} = q_n^{preh} \qquad \forall n \in N$$

(21)

where U^{preh} is the overall heat transfer coefficient and $lmtd_n^{preh}$ is the log mean temperature difference that is reformulated using Chen's approximation (Chen, 1987) to overcome the numerical difficulties created by the logarithm, in which, the temperature differences, θ, are given by **Eqs. (22-24).**

$$lmtd_n^{preh} = (0.5 \cdot (\theta_n^1 \cdot \theta_n^2)(\theta_n^1 + \theta_n^2))^{1/3} \qquad \forall n \in N$$

(22)

$$\theta_n^1 = T^{steam} - t_n^{memb} \qquad \forall n \in N$$

(23)

$$\theta_n^2 = T^{steam} - t_n^{hx,out} \qquad \forall n \in N$$

(24)

The temperature difference between shell and tubes must be greater than the design minimum difference temperature to allow effective heat transfer,

$$\Delta T^{min} \leq T^{steam} - t_n^{memb} \qquad \forall n \in N$$

(25)

$$\Delta T^{min} \leq T^{steam} - t_n^{hx,out} \qquad \forall n \in N$$

(26)

The same procedure, which is detailed in **Appendix A**, is applied to design the heat exchanger and cooler.

2.3 GDP formulation in membrane stages

To determine the number of distillation stages present in the desalination system, the disjunction showed in **Eq. (27)** is introduced to formulate the decision of the existence of a stage. If the stage exists, the concentrate stream of the previous stage, $f_{n-1}^{conc} = f_n^{feed}$, is equal to the inlet flowrate through stage *n*, f_n^{stage} (see **Fig.2**). Otherwise, f_n^{stage} is equal to zero and $f_n^{feed} = f_n^{bypass}$. In this equation, the Boolean variable: Y_n^{stage} will be «True» if the stage *n* exists and «False», otherwise.

$$\begin{bmatrix} Y_n^{stage} \\ F_n^{stage,LO} \leq f_n^{stage} \leq F_n^{stage,UP} \\ f_n^{bypass} = 0 \end{bmatrix} \veebar \begin{bmatrix} \neg Y_n^{stage} \\ F_n^{bypass,LO} \leq f_n^{bypass} \leq F_n^{bypass,UP} \\ f_n^{stage} = 0 \end{bmatrix} \forall n \in N \qquad (27)$$

$$Y_n^{stage} \in \{True, False\}$$

The previous disjunction can be reformulated into an MINLP model, by using the hull reformulation (Vecchietti et al., 2003) as follows:

$$\begin{aligned} & f_n^{stage} \leq F_n^{stage,UP} \cdot y_n^{stage} \\ & f_n^{stage} \geq F_n^{stage,LO} \cdot y_n^{stage} \\ & f_n^{bypass} \leq F_n^{bypass,UP} \cdot (1 - y_n^{stage}) \\ & f_n^{bypass} \geq F_n^{stage,LO} \cdot (1 - y_n^{stage}) \\ & y_n^{stage} \in \{1, 0\} \end{aligned} \qquad (28)$$

Some logical relationships (**Eqs. 29** and **30**) are included in the model, in terms of Boolean variables and their corresponding re-formulation to algebraic equations using

binary variables. See Raman and Grossmann (1994) for a detailed description of how to systematically transform logic propositions to algebraic equations.

Eq. 29 specifies that a membranes stage or a bypass must exist.

$$Y_n^{stage} \veebar Y_n^{bypass} \qquad \rightarrow \qquad y_n^{stage} + y_n^{bypass} = 1 \qquad \forall n \in N$$

(29)

If a bypass exists in stage *n*, then the bypass should also exist in all subsequent stages to avoid the non-existence of intermediate stages.

$$Y_n^{bypass} \Rightarrow Y_{n+1}^{bypass} \qquad \rightarrow \qquad y_n^{bypass} \leq y_{n+1}^{bypass} \qquad n < \left|N\right|$$

(30)

2.4 Objective function

The objective function to be minimized corresponds to the total annualized cost (TAC) of the multistage MDS. The TAC comprises the contributions related to the annualized capital investment (CAPEX) of the equipment (including membrane modules and heat exchangers), and the annual operational expenses (OPEX) associated with the cost of membranes replacement, pumping, heating, and cooling:

$$\min: \; tac = capex \cdot F + opex$$

(31)

In which, *F* is the annualization factor as defined by (Smith, 2005):

$$F \cdot \left((1+I)^W - 1\right)^{-1} = I \cdot (1+I)^W$$

(32)

where *I* is the interest rate per year and W is the time horizon.

The capital expenditure includes the membrane cost (C^{memb}) and the capital cost of the heat exchangers, which are calculated by the correlation proposed by Turton et al.

(2012). All capital costs have been updated for the relevant year by the CEPCI index (Chemical Engineering Plant Cost Index).

$$capex = C^{memb} \cdot a_n^{memb} + FBM \cdot \left[114.79 \cdot (a_n^{preh} + a_n^{hx} + a_n^{preh}) + 40,7914) \right] \quad (33)$$

In **Eq. (33)**, *FBM* corresponds to a correction factor which correlates the operating pressure with the construction material.

As aforementioned, the operational expenses (*OPEX*) include membrane replacement cost (C^{replac}), considered to be equal to 15% of the capital cost per year; pumping cost (C^{pumps}); heating cost (C^{steam}); and cooling cost (C^{water}).

$$opex = \sum_{n \in N} C^{memb} \cdot a_n^{memb} \cdot C^{replac} + (C^{steam} \cdot f_n^{steam} + C^{pumps} \cdot f_n^{pumps} + C^{water} \cdot q_n^{cooler}) \cdot WH \quad (34)$$

In **Eq. (34)**, WH is the working hours per year; f_n^{steam} is calculated from the total energy required and the water heat of vaporization, and f_n^{pumps} includes the process flows which need pumping.

3. Case studies initial data

Several case studies, based on real produced water data generated from the Marcellus shale formation, have been performed to evaluate the capabilities of the proposed mathematical model to optimize MDS applied to close to ZLD desalination of shale gas water.

The present work considers that the MDS has the capacity to treat the produced water generated by 3 wellpads of 12 wells each (Manda et al., 2014). Therefore, the input mass flowrate is equal to 2 $kg \cdot s^{-1}$ (7.22 $m^3 \cdot h^{-1}$), based on the maximum capacity per well (i.e $4.82 \cdot 10^{-2}$ $kg \cdot s^{-1}$ including 15% extra capacity).

The base case study considers Marcellus shale salinity of 200 $g \cdot kg^{-1}$ water since U.S. Environmental Protection Agency (2016) reported that produced water generated per well in the U.S ranges from $1.71 \cdot 10^{-2}$ $kg \cdot s^{-1}$ to $4.82 \cdot 10^{-2}$ $kg \cdot s^{-1}$ and Marcellus shale salinity average sampling data for 19 sites is 200 $g \cdot kg^{-1}$ water. Nevertheless, the produced water from different wells can have significant salinity differences depending on the shale gas formation. For this reason, sensitivity studies of the system behavior have been performed under different salt concentrations ranging from 150 to 250 $g \cdot kg^{-1}$ water. The MDS outlet concentrate salinity has to be greater or equal than 300 $g \cdot kg^{-1}$ water (i.e. close to salt saturation condition of ~ 350 $g \cdot kg^{-1}$ water) to maximize the water recovery. **Table 1** summarizes all the input data used in the case studies.

Table 1. Input data used in the model.

Feed water		**Source**
Mass flowrate	7.22 $m^3 \cdot h^{-1}$ (2 $kg \cdot s^{-1}$)	(Lira-Barragán et al., 2016)
Temperature	20 ºC	(Onishi et al., 2017b)
Membrane parameters		**Source**
Thickness	0.65 mm	(Al-Obaidani et al., 2008)
Permeability	5.6 10^{-3} kg $(m^2 \cdot Pa \cdot h)^{-1}$	(Lokare et al., 2017)
Output parameters		**Source**
Outlet Salinity	300 $g \cdot kg^{-1}$	(Onishi et al., 2017b)
Cost Data		**Source**
Cooling water cost	11.2 US$ $(kW \cdot year)^{-1}$	(Turton et al., 2012)
Steam cost a	0.007 US$ $\cdot kg^{-1}$	(Al-Obaidani et al., 2008)
Membrane cost	90 US$ m^{-2}	(Al-Obaidani et al., 2008)
Pumping cost	0.056 US$ m^{-3}	(Song et al., 2008)
Factor of annualized capital cost	0.13 (5% - 10 year)	
Factor of annualized	0.28 (5% - 4 year)	

Additionally, in order to ensure that the system works within its operational limits, the following variables have been fixed or constrained: 1) the membrane inlet temperature is restricted between 40 - 90 ºC; 2) minimum temperature difference between the shell and tubes in the heat exchanger is equal to 10 ºC; 3) cooler outlet temperature is fixed to 30 ºC to allow sufficient difference of vapor pressure at both sides of the membrane (i.e. membrane driving force) and 4) the use of water as refrigerant fluid (i.e. other refrigerant fluids have been discarded due to their higher comparative price (Turton et al., 2012)).

In the following sections, the main results obtained are described.

4. Results and discussion

4.1 Multistage membrane distillation design

The resulting optimal MDS configuration for the base case, using Marcellus real shale salinity of 200 $g \cdot kg^{-1}$ water, consists of three MD stages with a total required membrane area of 603 m^2 (225, 221 and 157 m^2, respectively). Additionally, a recycle ratio (total recycle flowrate with respect to the feed flowrate) of 9 allows reaching the outlet salinity specification (i.e. 300 $g \cdot kg^{-1}$ water). The optimum configuration and the main process variables (i.e. areas, flows, temperatures, utilities, etc.) are shown in **Fig. 5.**

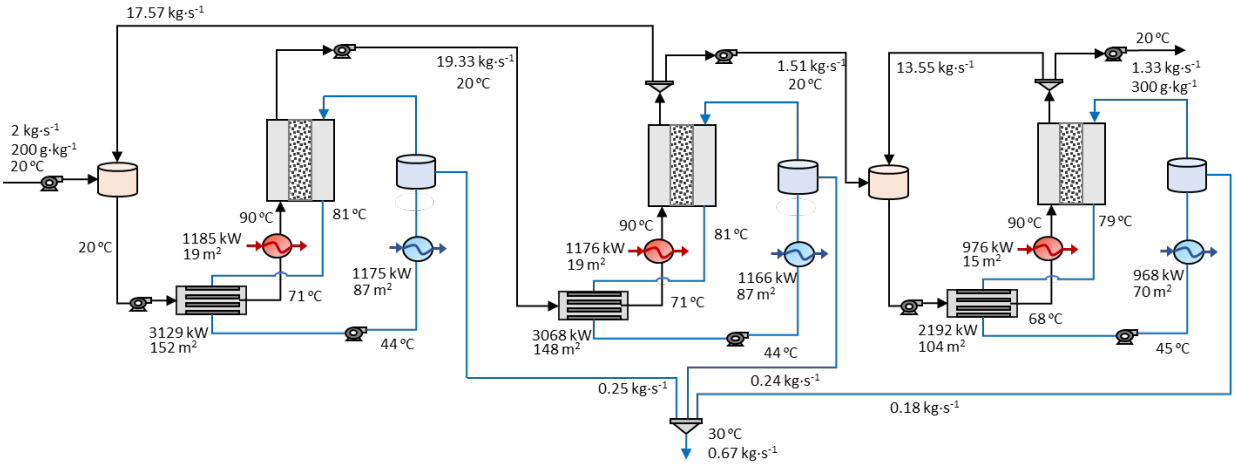

Fig. 5. Optimal solution of the multistage membrane distillation system (MDS) with heat integration obtained for the base case study.

The accuracy of the optimal solution obtained is verified using the commercial software Aspen HYSYS® (version 8.8) assuming steady state conditions and using the thermodynamic package NRTL-electrolytes. To simulate the MDS, the variables have been classified as process variables and design variables, being the design variables the input data needed to simulate the system (i.e. outlet temperature of heaters, coolers and heat exchangers, reject temperature and outlet salt concentration). A logical unit balance operation is used to simulate the energy and mass balances through the membrane. **Appendix B, Fig. B.1** shows the MDS diagram in Aspen HYSYS® and **Table B.1** the values of the process variables obtained from the mathematical model, from the simulation and the difference between them. For all variables, the differences found comparing both values are below 1%.

The optimal MDS solution achieves a total annualized cost (TAC) of 523 kUS$ year^{-1}, including 88 kUS$ year^{-1} related to capital expenditure and 435 kUS$ year^{-1} in operational expenses. **Fig. 6** shows the fractional contribution of various cost elements for the optimal solution. As can be observed, TAC mayor contributor is the heating energy required by the system (~ 62 %), followed by the pumping costs (~ 12 %). Since

high recycle ratios are needed to reach the outlet specified salinity and these streams must be reheated before entering the membrane stage again, the amount of thermal and pumping energy required increases dramatically. Similar findings were reported by Tavakkoli et al. (2017), in whose study most of the operational cost was attributed to the thermal energy requirements.

Optimal recycle configuration includes direct recycle in stage three while an inter-stage recycle between the second and first stages is established, obtaining the lowest overall recycle ratios.

To analyze the effect of the system configuration (i.e. the recycle connections and the number of MD stages) on the cost of the MDS, several cases have been solved varying these design variables.

Firstly, to study the influence of the recycle connections, the system has been solved predetermining different recycle configurations. The results for the CAPEX, OPEX and the heating cost, which is the maximum contribution to OPEX, are detailed in **Table 2**.

Table 2. Optimal costs (kUS$ year^{-1}) of MDS under different recycle connections.

Recycle ratio configuration description	CAPEX	OPEX	Heating cost
Direct recycle in each stage	88	452	310
Inter-stage recycle from stage three to stage one	87	466	343
Inter-stage recycle from stage three to stage two and direct recycle in stage one	88	440	321

If only direct recycle is allowed, the total cost increases 17 kUS$ year^{-1} with respect to the base case optimal solution. Considering inter-stage recycle from stage three to stage one, the operating cost increases 31 kUS$ year^{-1} compared with the optimal solution.

The solution of the last recycling possibility, inter-stage recycle from stage three to stage two and direct recycle in stage one, is only 5 kUS$ year^{-1} higher than the optimal solution. In all these three cases, higher recycle ratios than the obtained for the optimal solution are needed, and consequently, the resulting operating costs are higher.

As said before, the influence of the number of membrane distillation stages is also analyzed to find out the process cost differences compared to the optimal solution. The results, shown in **Fig. 7**, highlight that defining fewer stages than those calculated for the optimal solution is less attractive since a higher TAC is obtained. Although in these configurations (1 or 2 stages) the capital expenditure decreases, the operating costs rise to a larger extent, thus causing the increase of the TAC. When fewer membrane stages are used, higher recycle ratios are needed, consequently, the heating and pumping costs increase. For instance, when considering only one stage, although the capital cost is lower (58 kUS$ year^{-1}) due to the fewer installed equipment, the operational cost is 15 % higher than that in the optimal solution (500 kUS$ year^{-1}). On the contrary, the operational savings attained by adding more than three membranes do not compensate the capital cost increment (e.g., the capital cost is 132 kUS$ year^{-1} and the operational cost equal to 413.57 kUS$ year^{-1} considering six membranes in series).

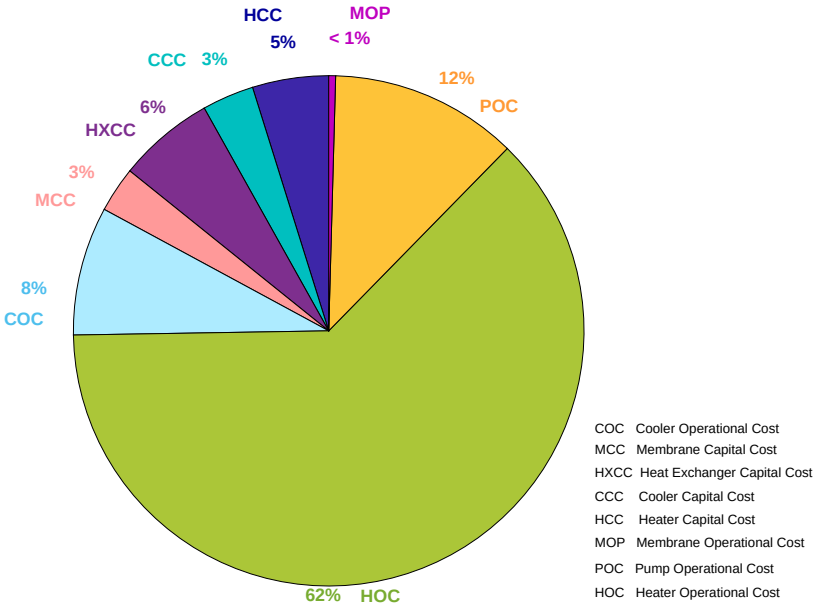

Fig. 6. Fractional contribution of various cost elements for the optimal solution of the base case study.

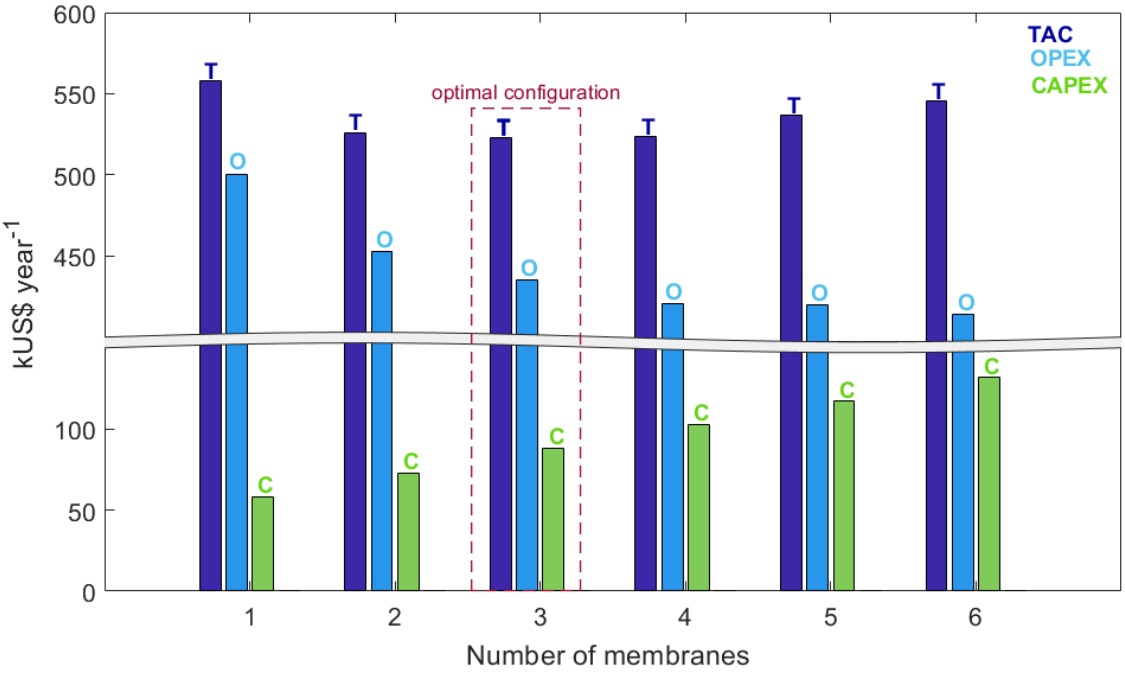

Fig. 7. Effect of the number of membrane stages in serires on the process cost.

4.2 Parametric study of the impact of membrane fouling

Membrane fouling is one of the major drawbacks in membrane technologies causing a severe flux decline, affecting the quality of the water and increasing the treatment costs.

Assuming that fouling affects the membrane permeability, we have solved the model for different permeability. Specifically, we have studied its effect on the capital and operational costs by decreasing its value by 10%, in a range from 90 to 50% of the permeability value used in the base case.

The results reveal that the TAC is slightly affected increasing the total cost by 8 kUS$ $year^{-1}$ comparing the base case with the worst situation (i.e. membrane permeability reduced by 50%). As the flux through the membrane decreases, to satisfy the salt concentration outlet requirement, both total membrane area and heating required increase from 603 to 697 m^2 and from to 3335 to 3379 kW. Hence, the results indicate that the membrane fouling have not a significant impact to the thermal efficiency of the process.

4.3 Parametric study of the effect of steam cost

As aforementioned, the TAC is significantly affected by steam cost. Some works in literature have considered the use of inexpensive heat sources such as the waste heat of process facilities or flaring (Bamu et al., 2017; Elsayed et al., 2015; Elsayed et al., 2014; González-Bravo et al., 2017, 2015). That consideration is very attractive for membrane distillation where the separation occurs below the normal water boiling point.

Taking into account that the steam cost varies significantly depending on the location of the plant and country, in this section we study the impact of the steam cost on the system configuration and total process cost. We analyze the base case, which considers low-cost steam equal to US$ 0.007 kg^{-1} (Al-Obaidani et al., 2008), and the extreme situations, considering a high-cost steam equal to US$ 0.028 kg^{-1} (Turton et al., 2012) and free heating source. In the latter case, the heating cost is removed from the objective function since the energy is provided from waste heat of shale gas production.

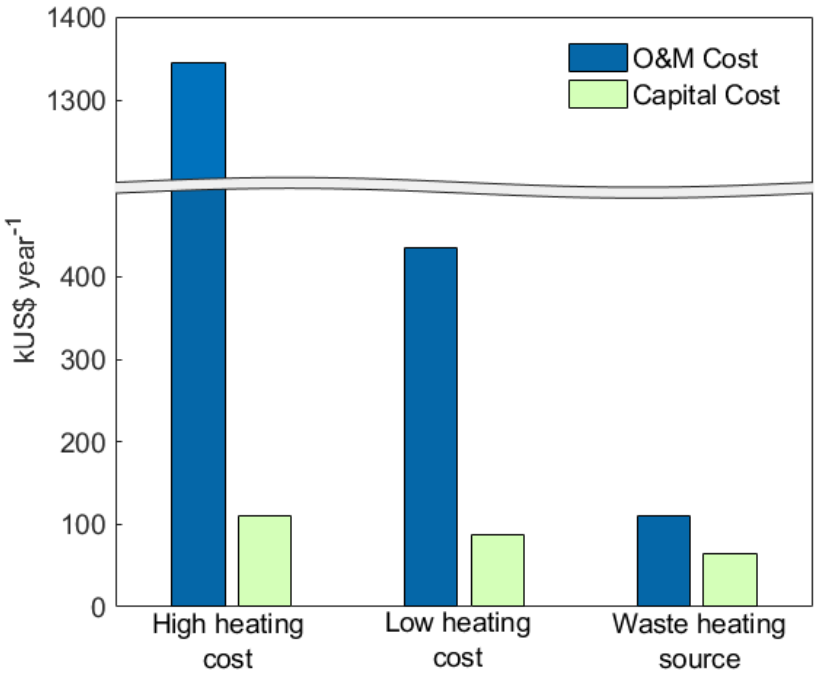

Fig. 8. Effect of steam cost on the total process cost for the optimal solution of the base case study.

Fig. 8 shows the capital and operation and maintenance (O&M) costs for the optimal solution of the three considered situations for the steam cost (inlet salinity in maintained constant at 200 g·kg^{-1} water). The TAC of treating produced water is equal to 1546 kUS$ year^{-1} considering high energy costs; 523 kUS$ year^{-1} for the base case (low heating cost); and 174 kUS$ year^{-1} when energy is provided from waste heat of shale gas production. The operational expenses take the value of 1345 kUS$ year^{-1}, 435 kUS$ year^{-1} and 65 kUS$ year^{-1}, respectively, which means that operational cost savings up to 95% could be obtained depending on the heating source. Although clearly the cost savings are affected by the heating cost reduction, they also arise from the differences in the system configuration. As can be seen in **Fig. 8**, the capital expenses also decrease as the heating cost is lower, being the system configuration equal to four, three and two stages, respectively. This is due to the trade-off between the amount of water recycled and the number of membrane stages. The higher the number of membrane stages, the

lower recycle ratios are needed. Therefore, when the heating cost is low, it is more cost-effective to preheat high recycle ratios than increase the number of membranes stages.

4.4 Parametric study of the effect of produced water salinity

The composition of the produced water is another uncertain parameter for designing MDS. It depends on the exploitation site and it varies also over the well lifetime.

In this section, the analysis of the optimal system configuration and economic performance of the system under different inlet salinities - ranging from 150 to 250 $g \cdot kg^{-1}$ water – is evaluated. Note that the outflow brine salinity remains up to 300 $g \cdot kg^{-1}$ water to achieve close to ZLD conditions and therefore, the maximum water recovery.

Fig. 9 shows the effect of the produced water salinity on treated water cost and desalinated water cost. In this figure, it is possible to observe that the treated water cost decreases when the inlet salinity increases, changing from 11.54 to 4.42 27 US$ per cubic meter of inlet water. This reduction in process costs occurs since, as the concentrations of inlet and outlet streams are more similar, less energy is needed to achieve the outflow stream near saturation conditions. Note that equipment size and the number of membrane modules are also reduced for treating feed water with higher TDS contents. For instance, the total membrane area for the MDS configuration, for the extreme salt concentrations (i.e., inlet concentration of 150 $g \cdot kg^{-1}$ water and 250 $g \cdot kg^{-1}$ water), decreases from 925 m^2 to 295 m^2, correspondingly. Also, in the case of inlet salinity equal to 150 $g \cdot kg^{-1}$ water, an optimal solution of four MD stages is obtained, while only two MD stages are required to achieve the desired outlet condition with the highest inlet salinity (250 $g \cdot kg^{-1}$ water).

It is worth mentioning that, the recovered water production rate is reduced when considering higher feed water salinities. The water recovered when the inlet salinity is significantly high (250 $g \cdot kg^{-1}$ water), decreases 67% comparing with the water

recovered when the inlet salinity is equal to 150 g·kg^{-1} water, thus increasing the amount of brine to be disposed. Hence, although the cost per cubic meter of inlet water decreases, the same cost expressed in terms of cost per cubic meter of permeate increases, changing from just over 23 US$ per cubic meter of water generated in the process to nearly 27 US$ per cubic meter. This trend agrees with works published by Elsayed, N et al. (2015) and Tavakkoli et al. (2017).

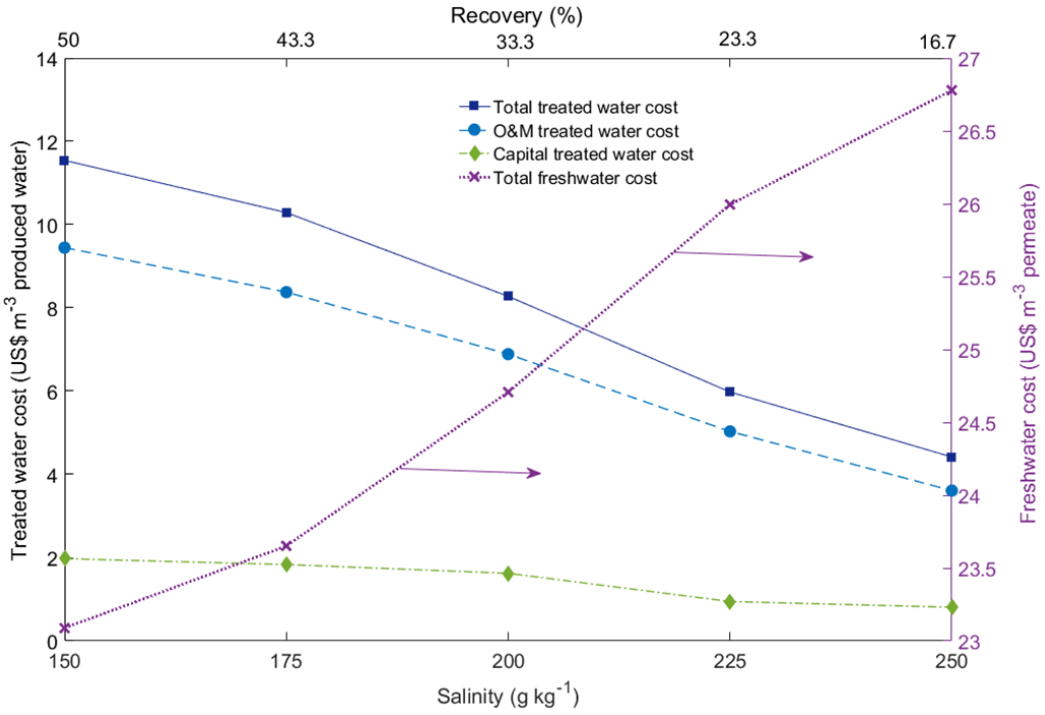

Fig. 9. Comparative effect of produced water salinity and water recovery on water treatment cost and freshwater cost of the multistage membrane distillation system.

4.5 Membrane distillation feasibility for treating shale gas produced water.

Previous sections highlighted the applicability of MDS to desalinate produced water to reach conditions close to ZLD. Nevertheless, the results indicate that the source of uncertainties such as the available heat source and inlet salinity conditions impact significantly the economic feasibility and configuration of MDS.

Without a low-cost steam source or waste heat available, the heating costs associated to obtain high permeate flux are significantly high. Whereas the steam source is usually known before deciding the selection of MDS as desalination technology, the reliability of the MDS design relies on the accuracy of the predicted value for the inlet salinity. On the one hand, if the MDS is designed for the worst case of the inlet salinity (lowest forecast value), the system will always satisfy the imposed specific salinity outlet conditions. However, this design would be at the expense of a high initial capital investment that might not be worthwhile if the real value (once the uncertainty is revealed) of the inlet salinity is significantly higher than the worst case value. On the other hand, a design of the MDS considering the mean forecast value requires a lower capital expenditure than the previous situation. Nevertheless, the specific outlet salinity may not be attained if the feed concentration is below the mean value.

As commented above, a comparison between the proposed MDS and a conventional thermal desalination technology used in shale gas operations, such as MEE-MVR (Silva et al., 2017) has been carried out. Onishi et al. (2017b) reported an optimal MEE-MVR treatment cost of 3.8 US$ m^{-3} of inlet water for an inlet salinity of 220 $g \cdot kg^{-1}$ water and inlet flowrate of 10.42 $kg \cdot s^{-1}$. As the MEE-MVR was designed for a higher flow rate, the treated cost is updated using the equation of the effect of the capacity on the equipment defined by Turton et al., 2012. **Table 3.3** summarizes the treated water cost obtained with both technologies considering three different inlet water salinity and inlet flow equal to 2 kg·s-^{1}.

Table 3. Treated water cost to desalinate shale gas water using MEE-MVR and MDS* (US$ per cubic meter shale gas water).

Shale gas water salinity ($g \cdot kg^{-1}$)	**MEE-MVR****	**MDS**	
		Low heating	**Waste heating**

		cost	source
70	9.9	15.4	5.5
150	9.4	12.4	4.1
200	7.8	8.2	2.7

* Results obtained by specifying brine salinity levels near to salt saturation concentration (i.e., 300 g kg^{-1}) and inlet flow equal to 2 $kg \cdot s^{-1}$.
** Updated cost using the equation of the effect of the capacity on the equipment defined by Turton et al., 2012

Clearly, if only heating source at high cost is available, MEE-MVR should be selected since the cost is significantly lower. If low heating cost is accessible, the decision is not trivial. Although the treated water cost using MD is higher than that obtained with MEE-MVR, it must be emphasized that the difference is smaller as the salinity increases. Additionally, as mentioned in the introduction section, it should be considered that nowadays flowback water, which salinity is lower, is directly reused to fracture other wells. Then, the water treated for discharge will be produced water (inlet salinity higher than 150 $g \cdot kg^{-1}$ water). Another important point that can influence the decision is that MEE-MVR requires a continuous electrical supply such as a power grid, which could be limited or unavailable in remote shale gas extraction sites. Besides, specialized equipment, such as electrical-driven compressors or flash tanks, is necessary. On the contrary, the inherent modular nature of MD is advantageous for produced water treatment, since its compactness and mobility facilitate the installation of small desalination plants near remote extraction sites. Moreover, MD can operate using low-grade industrial steam that can be easily obtained in shale gas operations from waste heat recovered from the process facilities or flaring. Additionally, the treating cost of MD using waste heat is approximately half of the cost obtained using MEE-MVR (see **Table 3.3**).

As shown in previous sections, the shale gas produced water treatment cost is very sensitive to many factors such as inlet and outlet conditions or heating cost. This fact, coupled with the lack of standardized methodologies for cost calculations, hinders the

economic comparison between MDS and other desalination technologies applied to this type of high salinity wastewater.

5. Computational aspects

The MINLP problem has 6 binary variables, 265 continuous variables and 311 constraints (263 equalities). The proposed MINLP model is implemented in GAMS software (version 24.7.1) and solved on a computer with a 3 GHz Intel Zeon Processor and 32 GB RAM running Windows 10. The solver ANTIGONE is used to optimize the problem. ANTIGONE is a deterministic mixed-integer non-linear-based global optimizer able to obtain global solution even for highly nonlinear and nonconvex character problems as the ones solved in this work. The problem required a CPU time of 628 s with 0% optimality gap. It should be highlighted that the bounds of all variables and good starting point are essential to solve the mathematical problem. As initial values we took the solution obtained solving the model fixing the structure of the system (i.e. the number of stages).

6. Conclusions

The present work highlights the potential for designing and deploying membrane distillation systems to treat shale gas produced water with high salt concentration. For this purpose, a multistage membrane distillation system (MDS) superstructure with energy recovery is modeled using the GDP framework as a MINLP problem in the GAMS modelling language. Then, this model is optimized to minimize the total annualized cost (TAC) of the system subject to the zero liquid discharge (ZLD) condition (i.e., a concentrate stream close to salt saturation conditions), which guarantees the maximum water recovery. It is worth noting that improving the cost-effectiveness of the process by reducing brine discharges decreases the water footprint associated with the shale gas production.

As a result, an optimal full-scale membrane distillation is designed to desalinate wastewater from shale gas operations by establishing the number of membrane modules in series, the size of heat exchangers, and the system operating conditions. Note also, the high complexity of the model, since the mass flowrates and temperatures of the streams are decision variables, and many of the equations that define the problem are non-convex and non-linear.

The results obtained emphasize the applicability of this promising technology, especially when a low-cost energy source or waste heat are available. The treatment cost varies significantly depending on the energy cost since it represents more than 50% of the total annualized cost. For example, the cost per cubic meter of treated water is 23.0 m^{-3} US$ for high energy costs; 8.3 m^{-3} US$ for low energy costs; and 2.8 m^{-3} US$ when energy is provided from waste heat of shale gas production.

Additionally, due to the uncertain salinity forecast of produced water, the reliability of the model has been checked by a sensitivity analysis carried out by varying the TDS

concentration from 150 to 250 g kg^{-1} water. The results reveal that the optimal configuration and the treatment cost depend significantly on the inlet salinity. Both the number of membrane stages and the total cost decrease as the inlet salinity increases. For the lowest value of salinity used in the analysis (i.e., 150 g kg^{-1} water), a cost of 11.5 US$ m^{-3} of inlet water is obtained with a system configuration composed of four membrane stages. On the contrary, for the highest salinity value (i.e., 250 g kg^{-1} water) both the cost and the number of membranes in the system decrease to 4.4 US$ m^{-3} of inlet water and two stages, respectively. Although the solutions considering higher feed water salinities are more cost effective, they have an important drawback for the water footprint of the shale gas exploitation activity. That is the low permeate flux of the MD process, which implies that only a small fraction of the huge amount of wastewater for the gas production is recovered.

The proposed model intends to be a systematic tool to guide the decision-maker towards the most cost-effective MDS design for this particular application. Although other economic analyses of MD applied to shale gas wastewater can be found in the literature, to the best of our knowledge, this is the first one that develops an MDS mathematical model coupled with heat recovery to determine the optimal design of the multistage structure and inter-stage recycling for several initial conditions obtaining the minimum cost.

Additionally, although MDS can be economically advantageous in remote areas where waste heat or low-grade thermal energy is available, and despite the advances made in the study of MD process, more laboratory analysis and pilot scale tests are still necessary to make this technology commercially attractive for shale gas wastewater desalination processes.

Further development of this work includes the design of multistage MDS coupled with solar thermal systems to find a robust design that ensures the optimal economic performance of the process during its entire lifetime whether there is enough, little or no waste energy available.

ACKNOWLEDGMENTS

 This project has received funding from the European Union's Horizon 2020 Research and Innovation Program under grant agreement No. 640979.

NOMENCLATURE

Roman letters

a	Area, m^2
B	Membrane permeability, kg $(m^2 \cdot Pa \cdot h)^{-1}$
CAPEX	Capital cost, kUS\$ $year^{-1}$
h	Specific enthalpy, $kJ \cdot kg^{-1}$
f	Mass flowrate, kg s^{-1}
F	Annualized capital cost factor
ht	Heat transfer coefficient, W m^{-2} K^{-1}
hv	Latent heat of vaporization of water, kJ kg^{-1}
I	Fractional interest rate per year
j	Vapor flux through the membrane, kg $m^{-2}h^{-1}$
$lmtd$	Logarithmic mean temperature difference
W	Horizon time, year

$OPEX$	Operational cost, kUS$ year^{-1}
p	Pressure, Pa
q	Heat flow, kW
t	Temperature, ºC
U	Overall heat transfer coefficient, kW (m^2 ºC)$^{-1}$
WH	Working hours in one year, h
x	Salt mass fraction
y	Binary variable
Y	Boolean variable

Superscripts

conc	Concentrate
cond	Conduction
hx	Heat exchanger
LO	Lower bound
m1	Membrane feed side
m2	Membrane permeate side
memb	Membrane
perm	Permeate
rec	Recirculated
refrig	Refrigerant
rej	Reject
UP	Upper bound

Subscripts

n	Membrane stage

Acronyms

CWT	Centralized Water Treatment
DCMD	Direct Contact Membrane Distillation
GAMS	General Algebraic Modelling System
GDP	Generalized Disjunctive Programming
MD	Membrane Distillation
MDS	Membrane Distillation System
MEE-MVR	Multiple-Effect Evaporation with Mechanical Vapor Recompression
MINLP	Mixed–Integer Nonlinear Programming
TAC	Total annualized cost
RO	Reverse Osmosis
TDS	Total Dissolved Solids
ZLD	Zero Liquid Discharge

Greek letters

θ	Temperature difference, ºC
γ	Activity coefficient of the water
ω	Salt molar fraction

REFERENCES

Al-Obaidani, S., Curcio, E., Macedonio, F., Di Profio, G., Al-Hinai, H., Drioli, E., 2008. Potential of membrane distillation in seawater desalination: Thermal efficiency, sensitivity study and cost estimation. J. Memb. Sci. 323, 85–98. doi:10.1016/j.memsci.2008.06.006

Ashoor, B.B., Mansour, S., Giwa, A., Dufour, V., Hasan, S.W., 2016. Principles and applications of direct contact membrane distillation (DCMD): A comprehensive review. Desalination 398, 222–246. doi:10.1016/j.desal.2016.07.043

Bamu, H., Abdelhady, F., Baaqeel, H.M., El-halwagi, M.M., 2017. Optimization of multi-effect distillation with brine treatment via membrane distillation and process heat integration. Desalination 408, 110–118. doi:10.1016/j.desal.2017.01.016

Carrero-Parreño, A., Onishi, V.C., Salcedo-Díaz, R., Ruiz-Femenia, R., Fraga, E.S., Caballero, J.A., Reyes-Labarta, J.A., 2017. Optimal Pretreatment System of Flowback Water from Shale Gas Production. Ind. Eng. Chem. Res. 56, 4386–4398. doi:10.1021/acs.iecr.6b04016

Chafidz, A., Kerme, E.D., Wazeer, I., Khalid, Y., Ajbar, A., Al-Zahrani, S.M., 2016. Design and fabrication of a portable and hybrid solar-powered membrane distillation system. J. Clean. Prod. 133, 631–647. doi:10.1016/J.JCLEPRO.2016.05.127

Chen, J.J.J., 1987. Comments on improvements on a replacement for the logarithmic mean. Chem. Eng. Sci. 42, 2488–2489. doi:10.1016/0009-2509(87)80128-8

Department of Enegy & Climate Change, 2013. The Unconventional Hydrocarbon Resources of Britain ’ S Onshore Basins - Shale Gas, Promote UK 2013.

Deshmukh, A., Boo, C., Karanikola, V., Lin, S., Straub, A.P., Tong, T., Warsinger, D.M., Elimelech, M., 2018. Membrane distillation at the water-energy nexus: limits, opportunities, and challenges. Energy Environ. Sci. doi:10.1039/C8EE00291F

Drioli, E., Ali, A., Macedonio, F., 2015. Membrane distillation: Recent developments and perspectives. Desalination 356, 56–84. doi:10.1016/j.desal.2014.10.028

Duong, H.C., Cooper, P., Nelemans, B., Cath, T.Y., Nghiem, L.D., 2015. Optimising

thermal efficiency of direct contact membrane distillation by brine recycling for small-scale seawater desalination. Desalination 374, 1–9. doi:10.1016/j.desal.2015.07.009

Elsayed, N., Barrufet, M., Eljack, F., El-Halwagi, M. 2015. Optimal Design of Thermal Membrane Distillation Systems for the Treatment of Shale Gas Flowback Water. Int. J. Membr. Sci. Technol. 2, 1–9. doi:10.15379/2410-1869.2015.02.02.01

Elsayed, N.A., Barrufet, M.A., El-Halwagi, M., 2014. Integration of thermal membrane distillation networks with processing facilities. Ind. Eng. Chem. Res. 53, 5284–5298. doi:10.1021/ie402315z

González-Bravo, R., Elsayed, N.A., Ponce-Ortega, J.M., Nápoles-Rivera, F., El-Halwagi, M.M., 2015. Optimal design of thermal membrane distillation systems with heat integration with process plants. Appl. Therm. Eng. 75, 154–166. doi:10.1016/j.applthermaleng.2014.09.009

González-Bravo, R., Ponce-Ortega, J.M., El-Halwagi, M.M., 2017. Optimal Design of Water Desalination Systems Involving Waste Heat Recovery. Ind. Eng. Chem. Res. acs.iecr.6b04725. doi:10.1021/acs.iecr.6b04725

Hammond, G.P., O'Grady, Á., 2017. Indicative energy technology assessment of UK shale gas extraction. Appl. Energy 185, 1907–1918. doi:10.1016/j.apenergy.2016.02.024

Hitsov, I., Maere, T., De Sitter, K., Dotremont, C., Nopens, I., 2015. Modelling approaches in membrane distillation: A critical review. Sep. Purif. Technol. 142, 48–64. doi:10.1016/j.seppur.2014.12.026

Jacquet, J.B., 2014. Review of risks to communities from shale energy development. Environ. Sci. Technol. 48, 8321–8333. doi:10.1021/es404647x

Kim, J., Kwon, H., Lee, S., Lee, S., Hong, S., 2017. Membrane distillation (MD)

integrated with crystallization (MDC) for shale gas produced water (SGPW) treatment. Desalination 403, 172–178. doi:10.1016/j.desal.2016.07.045

Lawson, K.W., Lloyd, D.R., 1996. Membrane distillation. I. Module design and performance evaluation using vacuum membrane distillation. J. Memb. Sci. 120, 111–121. doi:10.1016/0376-7388(96)00140-8

Lira-Barragán, L.F., Ponce-Ortega, J.M., Guillén-Gosálbez, G., El-Halwagi, M.M., 2016. Optimal Water Management under Uncertainty for Shale Gas Production. Ind. Eng. Chem. Res. 55, 1322–1335. doi:10.1021/acs.iecr.5b02748

Lokare, O.R., Tavakkoli, S., Khanna, V., Vidic, R.D., 2018. Importance of feed recirculation for the overall energy consumption in membrane distillation systems. Desalination 428, 250–254. doi:10.1016/j.desal.2017.11.037

Lokare, O.R., Tavakkoli, S., Rodriguez, G., Khanna, V., Vidic, R.D., 2017. Integrating membrane distillation with waste heat from natural gas compressor stations for produced water treatment in Pennsylvania. Desalination 413, 144–153. doi:10.1016/j.desal.2017.03.022

Lokare, O.R., Tavakkoli, S., Wadekar, S., Khanna, V., Vidic, R.D., 2017. Fouling in direct contact membrane distillation of produced water from unconventional gas extraction. J. Memb. Sci. 524, 493–501. doi:10.1016/j.memsci.2016.11.072

Manda, A.K., Heath, J.L., Klein, W.A., Griffin, M.T., Montz, B.E., 2014. Evolution of multi-well pad development and influence of well pads on environmental violations and wastewater volumes in the Marcellus shale (USA). J. Environ. Manage. 142, 36–45. doi:10.1016/j.jenvman.2014.04.011

OLI Systems, I., 2010. OLI ESP User Guide - A guide to using OLI ESP 8.2.

Onishi, V.C., Carrero-Parreño, A., Reyes-Labarta, J.A., Fraga, E.S., Caballero, J.A., 2017a. Desalination of shale gas produced water: A rigorous design approach for

zero-liquid discharge evaporation systems. J. Clean. Prod. 140, 1399–1414. doi:10.1016/j.jclepro.2016.10.012

Onishi, V.C., Carrero-Parreño, A., Reyes-Labarta, J.A., Ruiz-Femenia, R., Salcedo-Díaz, R., Fraga, E.S., Caballero, J.A., 2017b. Shale gas flowback water desalination: Single vs multiple-effect evaporation with vapor recompression cycle and thermal integration. Desalination 404, 230–248. doi:10.1016/j.desal.2016.11.003

Raman, R., Grossmann, I.E., 1994. Modelling and computational techniques for logic based integer programming. Comput. Chem. Eng. 18, 563–578. doi:10.1016/0098-1354(93)E0010-7

Rosenthal, R.E., 2016. GAMS — A User ’s Guide. GAMS Doc. 24.6. 1–316.

Ruyle, B., Fragachan, F.E., 2015. Quantifiable Costs Savings by Using 100 % Raw Produced Water in, in: SPE Latin American and Caribbean Petroleum Engineering Conference. Ecuador, p. 7.

Salcedo-Díaz, R., Ruiz-Femenia, R., Carrero-Parreño, A., Onishi, V.C., Reyes-Labarta, J.A., Caballero, J.A., 2017. Combining Forward and Reverse Osmosis for Shale Gas Wastewater Treatment to Minimize Cost and Freshwater Consumption, in: Computer Aided Chemical Engineering 40. pp. 2725–2730. doi:10.1016/B978-0-444-63965-3.50456-6

Shaffer, D.L., Arias Chavez, L.H., Ben-sasson, M., Romero-Vargas Castrillón, S., Yip, N.Y., Elimelech, M., Sha, D.L., Chavez, L.H.A., Ben-sasson, M., Castrillo, S.R., 2013. Desalination and Reuse of High-Salinity Shale Gas Produced Water: Drivers, Technologies, and Future Directions. Environ. Sci. Technol. 47, 9569–83. doi:10.1021/es401966e

Silva, T.L.S., Morales-Torres, S., Castro-Silva, S., Figueiredo, J.L., Silva, A.M.T.,

2017. An overview on exploration and environmental impact of unconventional gas sources and treatment options for produced water. J. Environ. Manage. 200, 511–529. doi:10.1016/j.jenvman.2017.06.002

Smith, R.M., 2005. Chemical Process Design and Integration. John Wiley and Sons, University of Manchester.

Song, L., Ma, Z., Liao, X., Kosaraju, P.B., Irish, J.R., Sirkar, K.K., 2008. Pilot plant studies of novel membranes and devices for direct contact membrane distillation-based desalination. J. Memb. Sci. 323, 257–270. doi:10.1016/j.memsci.2008.05.079

Swaminathan, J., Chung, H.W., Warsinger, D.M., Lienhard, J.H., 2016. Simple method for balancing direct contact membrane distillation. Desalination 383, 53–59. doi:10.1016/j.desal.2016.01.014

Tavakkoli, S., Lokare, O.R., Vidic, R.D., Khanna, V., 2017. A techno-economic assessment of membrane distillation for treatment of Marcellus shale produced water. Desalination 416, 24–34. doi:10.1016/j.desal.2017.04.014

Trespalacios, F., Grossmann, I.E., 2014. Review of Mixed-Integer Nonlinear and Generalized Disjunctive Programming Methods. Chemie Ing. Tech. 86, 991–1012. doi:10.1002/cite.201400037

Turton, R., Bailie, R.C., Whiting, W.B., Shaeiwitz, J.A., Bhattacharyya, D., 2012. Analysis , Synthesis , and Design of Chemical Processes, Fourth. ed. Prentice Hall.

U.S. Energy Information Administration, 2017. Annual Energy Outlook 2017. URL http://www.eia.gov/outlooks/aeo (accessed 3.12.18).

U.S. Environmental Protection Agency, 2016. Technical Development Document For Effluent Limitations Guidelines and Standars for the Oil and Gas Extraction Point Source Category. Washington, DC.

Vecchietti, A., Lee, S., Grossmann, I.E., 2003. Modeling of discrete/continuous optimization problems: characterization and formulation of disjunctions and their relaxations. Comput. Chem. Eng. 27, 433–448. doi:10.1016/S0098-1354(02)00220-X

Yang, L., Grossmann, I.E., Manno, J., 2014. Optimization models for shale gas water management. AIChE J. 60, 3490–3501. doi:10.1002/aic.14526

Yun, Y., Ma, R., Zhang, W., Fane, A.G., Li, J., 2006. Direct contact membrane distillation mechanism for high concentration NaCl solutions. Desalination 188, 251–262. doi:10.1016/j.desal.2005.04.123

Appendix A. Mathematical model

A.1 Mass and salt balances

Membrane distillation unit

Mass and salt balances around each membrane distillation are given by the following equations

$$f_n^{memb} + f_n^{rec} = f_n^{rec} + f_n^{perm} + f_n^{rej} \qquad \forall n \in N$$

(A.1.1)

$$f_n^{memb} \cdot x_n^{memb} = f_n^{rej} \cdot x_n^{rej} \qquad \forall n \in N$$

(A.1.2)

where, f_n^{memb}, f_n^{rec}, f_n^{perm} and f_n^{rej} represent the inlet mass flowrate, the recirculated flowrate, the permeate flowrate and the reject flowrate in the membrane module, respectively. x_n^{memb} and x_n^{rej} are the inlet and reject concentration in the membrane.

Recycle splitter

The possibility of various recycle connections is defined by the following equation:

$$f_n^{rej} = f_n^{recycle} + \sum_{\substack{n' \in N \\ n > n'}} f_{n,n'}^{recycle} + f_n^{conc} \qquad \forall n \in N$$

(A.1.3)

Where $f_n^{recycle}$, $f_{n,n'}^{recycle}$ and f_n^{conc} represent the direct recycle, the inter-stage recycles and the concentrate stream, respectively. The concentration, temperature and, consequently, the specific enthalpy of these streams are the same as for the reject stream.

Inlet mixer balances

The membrane inlet conditions are defined by the following mass, salt an energy balances around the inlet mixer placed before each membrane module.

$$f_n^{stage} + f_n^{recycle} + \sum_{\substack{n' \in N \\ n > n'}} f_{n,n'}^{recycle} = f_n^{memb} \qquad \forall n \in N \tag{A.1.4}$$

$$f_n^{stage} x_n^{feed} + f_n^{recycle} \cdot x_n^{rej} + \sum_{\substack{n' \in N \\ n > n'}} f_{n,n'}^{recycle} \cdot x_{n'}^{rej} = f_n^{memb} \cdot x_n^{memb} \qquad \forall n \in N$$

(A.1.5)

$$h_n^s(t_n^{feed}, x_n^{feed}) \cdot f_n^{stage} + h_n^s(t_n^{rej}, x_n^{rej}) \cdot f_n^{recycle} + \\ + \sum_{\substack{n' \in N \\ n > n'}} h_{n'}^s(t_{n'}^{rej}, x_{n'}^{rej}) \cdot f_{n,n'}^{recycle} = h_n^s(t_n^{hx,in}, x_n^{memb}) \cdot f_n^{memb} \qquad \forall n \in N$$

(A.1.6)

A.2 Permeate flux calculation

The permeate flux throughout the membrane is calculated as proposed by Elsayed et al. (2014),

$$j_n = B \cdot (p_n^{m1} \cdot \gamma_n (1 - \omega_n) - p_n^{m2}) \qquad \forall n \in N$$

(A.2.1)

in which, B is the membrane permeability, ω_n is the salt molar fraction in the feed side, γ_n represents the activity coefficient of the water in the feed side, and p_n^{m1} and p_n^{m2} are the vapor pressures at both sides of the membrane surface (see **Fig.3**). The salt molar fraction of the feed water is given by **Eq. (A.2.2).**

$$\omega_n \cdot (x_n^{memb} / 58.4 + (1 - x_n^{memb} / 18) = x_n^{memb} / 58.4 \qquad \forall n \in N$$

(A.2.2)

The activity coefficient is estimated as a function of the salt molar concentration by the following equation as proposed by Lawson and Lloyd (1996),

$$\gamma_n = 1 - 0.5 \cdot \omega_n - (10 \cdot \omega_n)^2 \qquad \forall n \in N$$

(A.2.3)

Vapor pressure is estimated with the correlation described in **Eq. (A.2.4),** which has been obtained using Antoine's equation for the range of the working temperatures (20 ºC - 90 ºC).

$$p_n = 16.56 \cdot (t_n)^2 - 935.90 \cdot t_n + 16960 \qquad \forall n \in N$$

(A.2.4)

A.3 Heat Exchanger and cooler design equations

The following equations and variables are used to model mathematically the heat exchanger and cooler. They can be described in four blocks of equations. The first one defines the energy balance across the equipment, the second one calculates the equipment area, in the third one Chen's approximation is applied to calculate the temperature difference and the last one ensures the workability of the equipment.

Heat Exchanger

Energy balance

$$\left(f_n^{rec} + f_n^{perm} \right) \cdot \left(h_n^p(t_n^{perm}) - h_n^p(t_n^{perm'}) \right) =$$
$$= f_n^{memb} \cdot \left(h_n^s(t_n^{hx,out}, x_n^{memb}) - h_n^s(t_n^{hx,in}, x_n^{memb}) \right) \qquad \forall n \in N$$

(A.3.1)

Heat exchanger area calculation

$$a_n^{hx} \cdot U^{hx} \cdot lmtd_n^{hx} = q_n^{hx} \qquad \forall n \in N$$ (A.3.2)

Chen's approximation for the calculation of logarithmic mean temperature difference

$$lmtd_n^{hx} = (0.5 \cdot (\theta_n^3 \cdot \theta_n^4)(\theta_n^3 + \theta_n^4))^{1/3} \qquad \forall n \in N$$ (A.3.3)

$$\theta_n^3 = t^{perm} - t_n^{hx,out} \qquad \forall n \in N$$ (A.3.4)

$$\theta_n^4 = t_n^{perm'} - t_n^{hx,in} \qquad \forall n \in N$$ (A.3.5)

Design temperature constraints

$$\Delta T^{min} \le t^{perm} - t_n^{hx,out} \qquad \forall n \in N$$ (A.3.6)

$$\Delta T^{min} \le t_n^{perm'} - t_n^{hx,in} \qquad \forall n \in N$$ (A.3.7)

Cooler

Energy balance

$$q_n^{cooler} = f_n^{rec} \cdot \left(h_n^p(t_n^{perm'}) - h_n^p(t_n^{rec}) \right) \qquad \forall n \in N$$ (A.3.8)

Area calculation

$$a_n^{cooler} \cdot U^{cooler} \cdot lmtd_n^{cooler} = q_n^{cooler} \qquad \forall n \in N$$ (A.3.9)

Chen’s approximation for the calculation of logarithmic mean temperature difference

$$lmtd_n^{cooler} = (0.5 \cdot (\theta_n^5 \cdot \theta_n^6)(\theta_n^5 + \theta_n^6))^{1/3} \qquad \forall n \in N$$ (A.3.10)

$$\theta_n^5 = t_n^{perm'} - T^{refrig,out} \qquad \forall n \in N$$ (A. 3.11)

$$\theta_n^6 = t_n^{rec} - T^{refrig,in} \qquad \forall n \in N$$ (A. 3.12)

Design temperature constraints

$$\Delta T^{min} \leq t_n^{perm'} - T^{refrig,out} \qquad \forall n \in N$$ (A. 3.12)

$$\Delta T^{min} \leq t_n^{rec} - T^{refrig,in} \qquad \forall n \in N$$ (A. 3.13)

Appendix B. Aspen Hysys® flow diagram and comparison between mathematical model and simulated results.

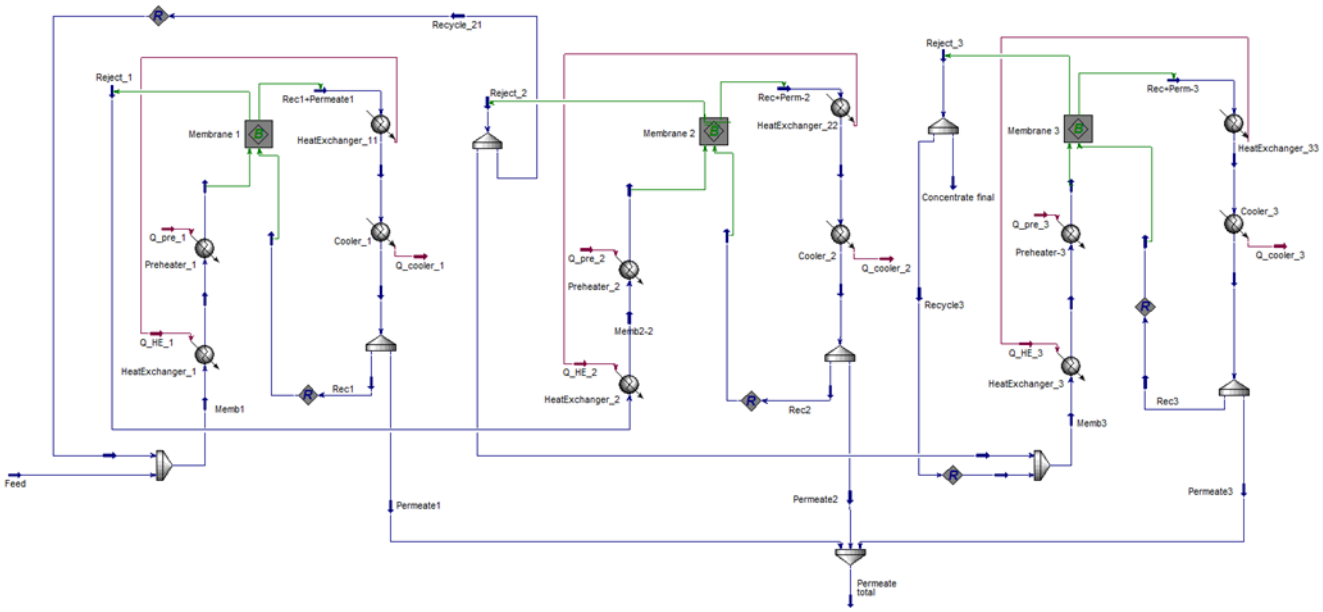

Fig. B.1 Membrane distillation system process flow diagram in Aspen HYSYS® of the optimal solution for the base case.

Table B.1 Process variables for the optimal solution of the MDS model and values obtained from the simulation.

Process Variables	Stage	Model	Hysys	Relative error (%)
Heat flow preheater (kW)	1	1185	1191	-0.50
	2	1176	1183	-0.59
	3	976	986	-1.01
Heat flow heat exchanger (kW)	1	3130	3113	0.54
	2	3068	3053	0.49
	3	2192	2186	0.27
Heat flow cooler (kW)	1	1175	1181	-0.51
	2	1166	1173	-0.60
	3	968	977,90	-1.01
Permeate temperature (ºC)	1	80.78	80.69	0.11
	2	80.60	80.50	0.12
	3	78.44	78.52	-0.10
Final concentrate ($kg \cdot s^{-1}$)	-	1.33	1.33	0.00
Final permeate ($kg \cdot s^{-1}$)	-	0.66	0.66	0.00